Classification
Physics Abstracts
61.40 — 61.12E

Small-angle neutron scattering in model porous systems : a study of fractal aggregates of silica spheres

Marie Foret, Jacques Pelous and René Vacher

Laboratoire de Science des Matériaux Vitreux (*), Université de Montpellier II, F-34095 Montpellier Cedex, France

(*Received 30 December 1991, accepted 13 February 1992*)

Abstract. — Porous solids built of fractal clusters can be obtained by destabilization of quasi-monodisperse silica sols. Small-angle neutron scattering, associated with transmission-electron microscopy, was used for a structural investigation of these aerogels in a broad length scale. We present a quantitative analysis of the data for materials with different particle sizes and polydispersities. The analysis of the wavevector region corresponding to the crossover between surface and volume scattering is especially emphasized.

1. Introduction.

The study of the structure of inhomogeneous systems by light, X-ray, and neutron scattering is a matter of considerable scientific interest. The most famous approach proposed by Guinier [1] describes the elastic scattering of X-rays as the sum of the intensities scattered by individual particles. The method is commonly used for the characterization of solutions and of porous aggregates of particles.

More recently, scattering techniques were used for the investigation of the structure of complex systems such as polymers [2] and gels [3]. In the following, we will restrict our discussion to structures obtained by the sol-gel route. In such materials, two important length scales should be distinguished. The first is related to the elementary blocks, which are generally more or less homogeneous particles, of average size r_0. These particles assemble to form inhomogeneous clusters, up to a correlation length ξ. In the range of length ℓ, $r_0 < \ell < \xi$, a large number of gels exhibit a fractal structure. At scales larger than ξ, these materials can be described as an almost homogeneous packing of clusters. Correspondingly, three distinct regimes are observed in the wavevector dependence of small-angle X-ray (SAXS) and neutron (SANS) scattering intensities, $I(q)$. At small q, $q\xi < 1$, in the so-called Guinier regime, $I(q)$ is weakly dependent of q. The power-law dependence, $I(q) \propto q^{-D}$, observed for $1/\xi \ll q \ll 1/r_0$ is the signature of a fractal structure, with a fractal dimension D. At larger q values, $qr_0 \gg 1$, the scattering originates from the surface of the particles : the Porod regime, $I(q) \propto q^{-4}$, is observed.

(*) URA CNRS n° 1119.

The main difficulty in the theoretical models is the description of the behaviour near the crossovers between the three above regimes. Several approaches have been proposed [4, 5], and have been used successfully to describe measurements on protein solutions [6] and fumed silica aggregates [5]. However, experimental observations such as the shape of the Guinier-to-fractal crossover in base-catalyzed silica aerogels [7, 8], as well as the crossover between fractal and Porod regions in colloidal gold aggregates [9] cannot be satisfactorily described by the above theories. Also, the question of the relation between the value of q at the latter crossover and that of r_0 is still open, especially in polydisperse systems.

In this paper, we present experimental data on a well-characterized model system of silica aerogels. Such materials, which are highly-porous single-phase solids, are ideally suited for structural studies of inhomogeneous media. The SANS data will be compared to electron-microscopy results, and fits to the theoretical expressions will be attempted in a range of q covering the three above regimes. In the discussion, we will show that modified forms of the above models have to be taken into account to allow a better description of the crossovers.

2. Sample preparation and characterization.

The silica gels were prepared by destabilization of commercial solutions (Ludox, trade mark of E. I. DuPont de Nemours & Co.). In these solutions, spherical particles of dense amorphous silica are dispersed in an alkaline-water solvent. The stability of such aquasols results from the negative charge of silica spheres, due to the small amount of sodium ions. We used three different sols of quasi-monodisperse particles, hereafter referred to as SM, LS, and TM, with nominal particle radii r_0 of 4, 7.5, and 12 nm, respectively. The sol is destabilized by decreasing the pH-value to 5.5. Several samples are prepared simultaneously from the same sol diluted with various amounts of ethanol, in order to obtain different densities of the final gels. Gelation occurs in a drying oven at 60 °C. The gelation time varies with silica concentration and particle diameter. At that stage, the solvent in the wet gel is a mixture of water and ethanol. In order to obtain an aerogel, we further process the gel following Kistler's method [10]. The wet gel is first washed with pure ethanol and then supercritically dried. In this way, we have prepared three series of low-density samples, each of them having different particle sizes. The densities range from 70 to 400 $kg.m^{-3}$

In order to increase the microstructure range of dry gels in a given series, was also prepared « xerogels » from the same wet material. In this case, the solvent is allowed to evaporate slowly, in ambient conditions. In contrast to supercritical drying, the gel is then submitted to capillary forces which induce profound changes in the structure of the solid skeleton. The main effect is a shrinkage which leads to macroscopic densities of about 1 000 $kg.m^{-3}$.

Transmission electron microscopy (TEM) observations were performed using a Jeol 200CX instrument. The specimens studied were small pieces of aerogel obtained by crushing, and deposited on a carbon-coated copper grid. Thin regions of the aerogel transparent to electrons were imaged in the microscope. A typical micrograph is shown in figure 1. The sample, of bulk density 250 $kg.m^{-3}$, shows the structure of a very tenuous aggregate of spheres, with an average radius $r_0 \simeq 13.5$ nm. The polydispersity is small, $\Delta r_0 \simeq 2.5$ nm. It is clear in the figure that the spherical shape of the sol particles is preserved in the aggregates which constitute the aerogel. It must also be noted that the connection between spheres is done through narrow necks.

In the case of these colloidal aerogels, TEM provides clear structural information at the particle scale. This makes these materials a very interesting model system for the interpretation of elastic scattering experiments.

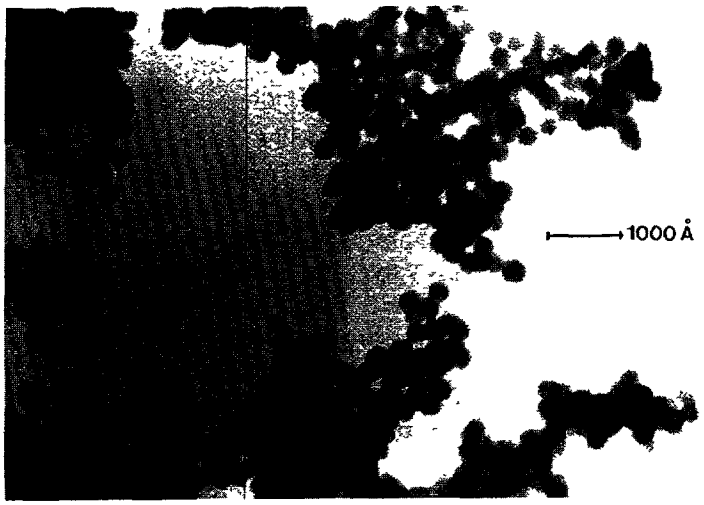

Fig. 1. — Transmission electron microscopy picture from a TM colloidal aerogel of density 250 kg.m^{-3} A mean radius $r_0 = 13.5$ nm and a polydispersity $\Delta r_0 = 3$ nm, defined as the difference between the largest and the smallest radius observed, are obtained.

3. Summary and discussion of theoretical predictions.

The theoretical description of the whole scattering curve must be made by calculating the space-Fourier transform of the density-density correlation function of the structure. This is in general a very difficult task, even on rather simple fractal models.

In the classical formulation [11] established for isotropic disordered systems of identical spherical particles, the intensity $P(q)$ scattered by one element is calculated first from the Fourier transform of $\rho(r)$, the scattering-length-density distribution :

$$F(q) = \int_0^{r_0} \rho(r) \frac{\sin(qr)}{qr} 4\pi r^2 \, dr \,. \tag{1}$$

The so-called form factor for an homogeneous particle ($\rho(r) = \rho$) is then obtained from the square of $F(q)$:

$$P(q) = V_0^2 \rho^2 \left[3 \frac{\sin(qr_0) - qr_0 \cos(qr_0)}{(qr_0)^3} \right]^2 , \tag{2}$$

where V_0 is the particle volume. The second step consists in evaluating the Fourier transform $S(q)$ of the pair-correlation function $g(r)$ of particles, each of them being assimilated to a point scattering an intensity $P(q)$. Following reference [4], in a fractal, $g(r)$ can be written as :

$$g(r) \propto \frac{1}{r_0^D} r^{D-3} \exp(-r/\xi) \,. \tag{3}$$

Here ξ is a fractal persistence length, which is introduced phenomenologically. From equation (3) and a proper normalization of $g(r)$, one gets [4]

$$S(q) = 1 + \frac{1}{(qr_0)^D} \frac{D\Gamma(D-1)}{\left(1 + \frac{1}{q^2\xi^2}\right)^{(D-1)/2}} \sin\left[(D-1)\,\mathrm{tg}^{-1}(q\xi)\right] , \tag{4}$$

where Γ is the gamma-function. The intensity scattered by a fractal assembly of N particles can now be written as :

$$I(q) \propto NS(q)\,P(q)\,. \tag{5}$$

A typical example of calculation of $I(q)$ is shown as the dashed-dotted line in figure 2. As far as $\xi \gg r_0$, the three above-discussed power-law regimes are observed, and the two corresponding crossovers occur near $q_\xi = 1/\xi$ and $q_{r_0} = 1/r_0$, respectively. The oscillations at large q are due to the form factor. Equation (5) has been used successfully, in particular to describe the fractal region and the crossover to homogeneity (see, e.g., Refs. [6, 8]). However, it must be noted that, in the vicinity of q_ξ, $I(q)$ in equation (5) can only decrease with increasing q. Thus, this description cannot account for the bump observed in base-catalyzed aerogels [7, 8]. This bump must originate from correlation effects in an assembly of clusters of average size ξ. Such interferences are not included in the above formulation of $g(r)$ [12]. A similar difficulty occurs in the analysis of data near q_{r_0}. As the particles are treated as « point » scattering sources instead of solid elements of finite size r_0, interference effects in the vicinity of q_{r_0} are neglected. A treatment of this problem has been proposed by Sinha and collaborators [9]. The amplitude of the « fractal » term in equation (3) is taken as an adjustable parameter. This is done formally by replacing r_0 in the normalization factor of equation (3) by an adjustable parameter r_f. These authors also included in $g(r)$ additional terms describing the pile-up of hard spheres. In this case, $g(r)$ is set equal to 0 for $0 < r < 2\,r_0$. The main new element of the model is a correlation between spheres introduced through a δ-peak at $2\,r_0$:

$$g(r) = \frac{V}{N}\,(z_1/16\,\pi r_0^2)\,\delta(r - 2\,r_0)\,. \tag{6}$$

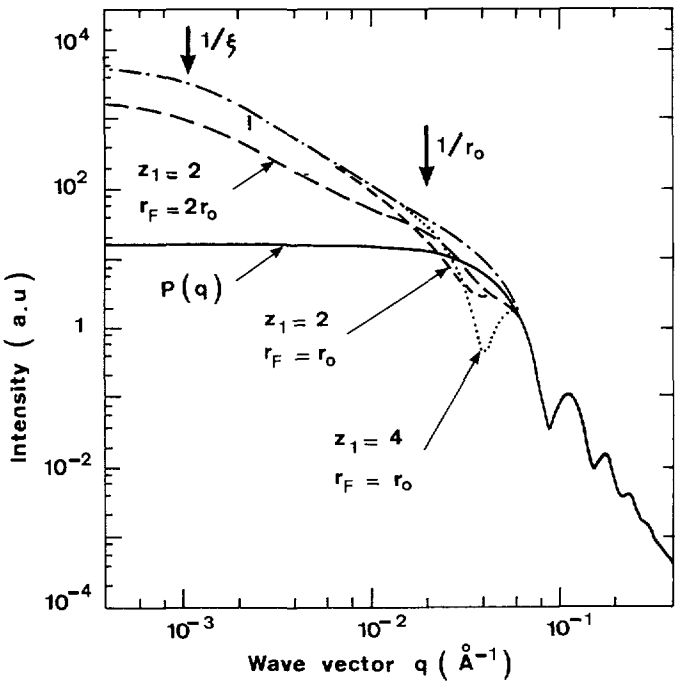

Fig. 2. — Calculation of the wavevector dependence of the scattered intensity in a SANS experiment from equation (5) (dashed-dotted line), and from the model of reference [9] with different parameter values. The solid line represents the form-factor contribution, equation (2).

Here, V is the scattering volume, and z_1 is the average coordination number of particles in the first shell. Several examples of calculations of $I(q)$ according to this model with different values of the parameters are shown in figure 2. The main difference with the results obtained from equation (5) above is the appearance of a dip near q_{r_0}. As expected, this dip becomes sharper, and shifts to larger values of q with increasing coordination number. The larger-order oscillations introduced by the Fourier transform of the δ-peak (Eq. (6)) match those of the form factor, as shown in figure 2. On the other hand, the effect of the factor multiplying the « fractal » term of $g(r)$ is to change the amplitude of $I(q)$ at $q < q_{r_0}$. It also shifts the value of q at which $S(q)$ departs from the fractal-power-law behaviour at large q's. In spite of the above improvement of the model, some departures of the fitting line from experimental data are still observed in figure 1 of reference [9], for values of $q > q_{r_0}$.

In the following, we will present an analysis of SANS data on colloidal solutions, aerogels and xerogels having very different structural characteristics. In particular, we will concentrate on the description of these results in the high-q region.

4. Experimental results and discussion.

SANS experiments were performed on the PAXE spectrometer at the Laboratoire Léon Brillouin in Saclay, France. We used a combination of two incident wavelengths and two sample-to-detector distances in order to cover the q-range from 3×10^{-3} to 0.3 Å^{-1}. The data were corrected from background and empty-cell contributions, and normalized by the spectrum of a purely-incoherent scatterer, which was water in this case. This also provided a correction for detector efficiency.

SANS data in colloidal aerogels give clear evidence for the experimental behaviours described in section 3. A log-log plot of the results for the lightest and heaviest samples of each aerogel series is shown in figure 3. In the small-q region, the Guinier regime is observed for the heaviest samples. At larger q, the power law $I(q) \propto q^{-D}$ extends over about one order of magnitude for the three low-density samples. This indicates a fractal structure, with $D \simeq 1.8$, independent of the size of the primary particles. The analogy of this value of D with that obtained by numerical simulations of diffusion-limited cluster-cluster aggregation [13, 14] suggests that this mechanism dominates the gelation process in colloidal aerogels. As already observed on different aerogels [8], the extension of the fractal range decreases with increasing density. The departure from the power-law behaviour, indicated by the arrows on the figure, shifts to larger q with decreasing particle diameter. The oscillations predicted by equation (2) are observed in the large-q region. In this regime, the similarity between $I(q)$ for samples of different densities belonging to the same family is evident. In contrast, the amplitude of the oscillations is very different for the different families of samples. This is related to the polydispersity of the particle sizes, which increases with decreasing r_0, as known from TEM measurements (Tab. I).

To start with a quantitative analysis, figure 4 shows the comparison of SANS data obtained with several samples prepared from the same TM sol. In the diluted sol, the silica particles can be assumed to scatter neutrons independently. Thus, the upper curve of figure 4 was fitted to the calculated form factor, equation (2). The best fit is shown as a solid line. The parameters are $r_0 = 13.5$ nm and $\delta r_0 = 1.6$ nm, and an amplitude coefficient. The small departure of the fit from the experimental data at small q is a signature of correlation effects between adjacent particles. The same calculated curve, shifted vertically to adjust the amplitude coefficient, has been compared to the three other experimental data sets. The excellent agreement at large q shows that the size, the shape, and the dispersity of the particles are conserved in the concentrated sol as well as in the dry gels. The main effect of the higher density in the

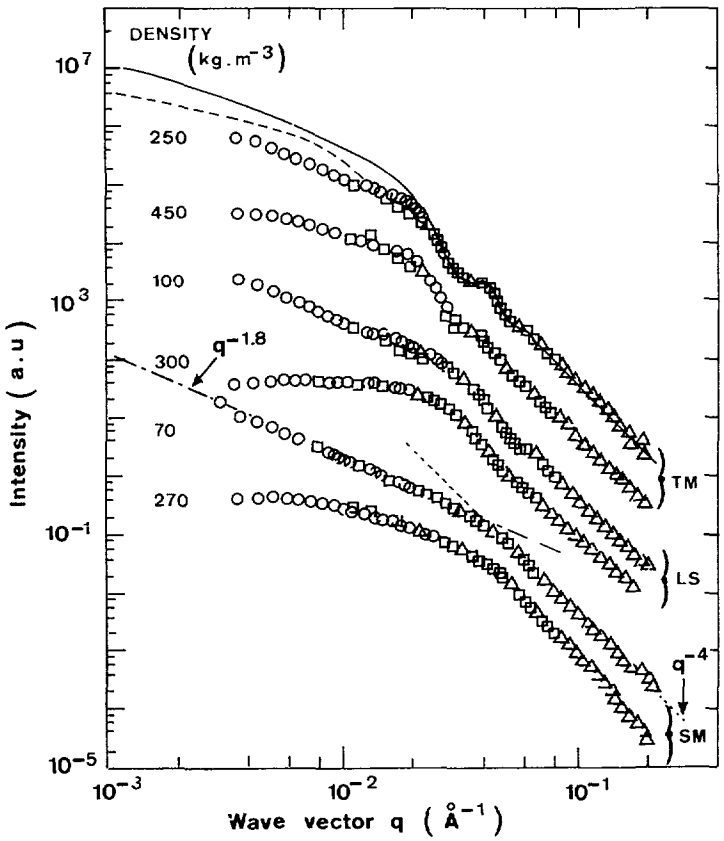

Fig. 3. — SANS results for the samples corresponding to the two extreme densities of each series. The solid and dashed lines are calculated as explained in the text. For the latter, the values $z_1 = 2$ and $r_f = 2\,r_0$ were used. The curves have been vertically shifted for clarity. Different symbols refer to distinct configurations of the spectrometer.

Table I. — *Sample parameters obtained by SANS and TEM.*

	SANS fitting parameters					TEM determination		
	α	β	D	r_0 (nm)	δr_0 (nm)	r_0 (nm)	Δr_0 (nm)	$q_\chi \cdot r_0$
TM	0.76	5.0	1.8 fixed	13.5	1.6	13.5	3	2.2
LS	0.70	4.2	1.8 fixed	8	1.4	8	2.5	2
SM	0.78	4.7	1.82 fitted	4.8	1.4	4.5	2.5	1.7

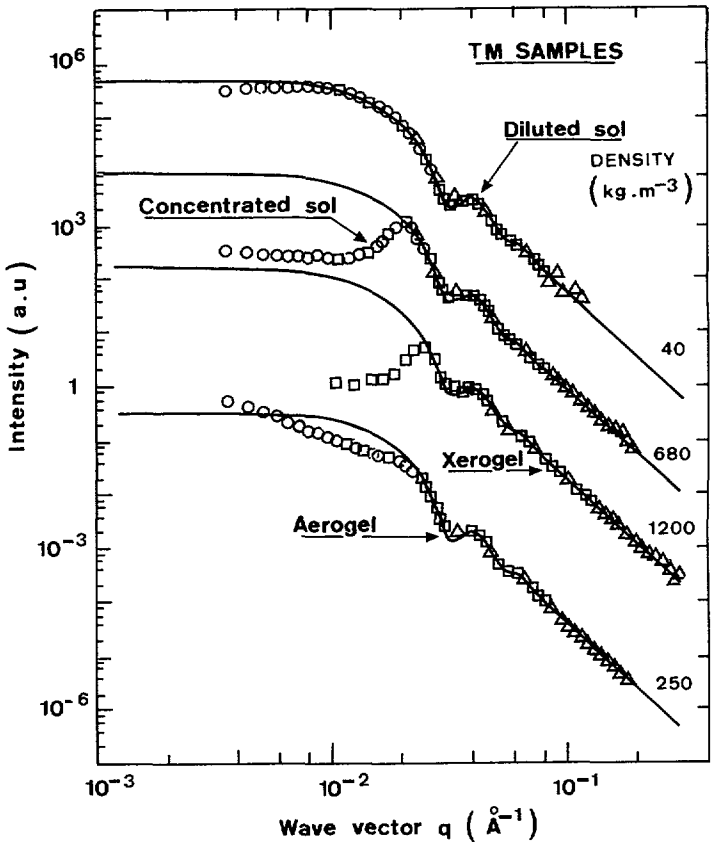

Fig. 4. — SANS results for TM samples in the sol and gel states. The solid line is a fit of the upper experimental curve to equation (2). Symbols are as in figure 3.

concentrated sol and in the xerogel is a drop of the intensity at small q due to interferences, resulting in a peak near q_{r_0}. This peak shifts to higher q with increasing density. For the aerogel, the power law associated to the fractal structure is observed on the left-hand side of the curve. It must be noted that, even in this case, the calculation of the form factor is larger than the experimental $I(q)$ near q_{r_0}. Thus, as the structure factor in equation (4) is always larger than 1, it is clear that a satisfactory fit of the whole curve by equation (5) cannot be obtained, as could be expected from the discussion in section 3. The above point is illustrated by a comparison of the solid line in figure 3, to $I(q)$ results for the lightest TM sample. As the values of r_0 and δr_0 are fixed by the fit of the form factor to the high-q region of the curve, the only adjustable parameters in equation (4) are D and ξ. The observation of a power-law dependence of $I(q)$ down to the lowest values of q investigated shows that ξ has little influence on the intensity curve. On the other hand, D was taken equal to 1.8 from the slope of the straight line. Other values of D do not improve the fit.

The result of one attempt at describing the same data following the method of reference [9] is shown as a dashed line in figure 3. The presence of an amplitude parameter in the « fractal » term improves the adjustment in the low-q region. However, as far as reasonable values are assumed for the coordination number z_1, an oscillation which is not present in the experimental data is observed in the calculated curve near q_{r_0}. This peak is associated to the

first-shell coordination term in $g(r)$ given in equation (6). This formulation assumes a single value of r_0, and z_1 is also taken as an adjustable constant. In fact, in addition to the distribution of r_0 due to particle polydispersity, z_1 is always widely distributed in a random fractal. This is clearly illustrated in figure 1 for the aerogel. Introducing a distribution of these quantities from site to site would result in a modulation of both the position and the amplitude of the oscillation in $I(q)$.

In our opinion, a more precise description of the data in the q_{r_0}-region would imply a better knowledge of $g(r)$ in this length domain. In disordered materials, this is obviously a very difficult task, and can only be solved empirically at this time. The main effect observed experimentally either on concentrated solutions or on dry gels being a drop of intensity at $q < q_{r_0}$, we have fitted our data by introducing in equation (5) an additional factor of the form : $1 - \alpha \exp[-(qr_0/\pi)^{\beta}]$. Here, α is linearly related to the amplitude parameter of the « fractal » term in the formulation of reference [9]. The exponent β governs the shape of the amplitude variation near q_{r_0}. Interferences due to the finite size of the particles can be the physical origin of the intensity dependence described by the above expression. Obviously, such a factor can only be used near q_{r_0}, as the interferences are properly accounted for at small q in equation (4). The recourse to it is justified here by the limited extension of the data below q_{r_0}. It must also be noted that the amplitude coefficient of the surface-scattering term in equation (3), as well as that of the « fractal » term in equation (4) are calculated for an assembly of *N isolated* particles. Thus, the need for a different intensity coefficient in the low-q and high-q region could possibly be related to a change in the surface-to-volume ratio

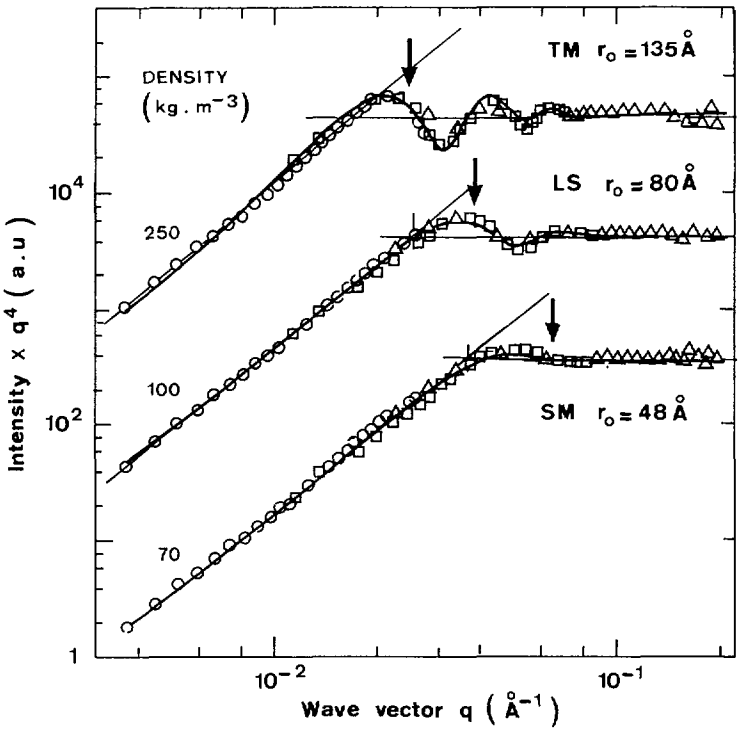

Fig. 5. — Log-log plot of $I(q) \times q^4$ for three colloidal samples, emphasizing the details of the volume-to-surface crossover, and the oscillations at large q. The arrows indicate the value $q = \pi/r_0$ for each sample. The intercept between the q^{-D} and q^{-4} lines defines the value of q_x.

between isolated and interconnected elements. Both effects above may occur simultaneously.

The results of fits using equation (5) modified by the above factor are shown in figure 5. To emphasize the oscillations, the data are plotted as log $(I \times q^4)$ *vs.* log q. The details of the curves are now well described. A value of D close to 1.8 is obtained. As shown in table I, the fits give for all the curves almost constant values of the parameters α and β, demonstrating that the nature of the crossover near q_{r_0} is sample independent, and likely related to one of the intrinsic mechanisms proposed above. The result $\alpha \simeq 0.7$ corresponds to $r_f \simeq 2\, r_0$. In view of the arguments used in reference [4] to calculate the amplitude of the fractal term, this is an indication that the fractal scaling of mass starts at a length scale corresponding approximately to $2\, r_0$.

Finally, we want to discuss the position of the surface-to-volume crossover, which is often used to determine an average particle size in gels. For an aggregate of well-defined monodisperse particles, this crossover can be expected to occur when the neutron wavelength is close to the particle diameter, $q \simeq \pi/r_0$. This value is shown as an arrow for three aerogels with different particle sizes in figure 5. For the quasi-monodisperse TM samples, the arrow is reasonably close to the point where the experimental data depart from the $I(q) \propto q^{-D}$ line. With increasing polydispersity, this departure occurs at smaller values of qr_0. If we define the crossover as the value q_χ where the extrapolations of the q^{-D} and q^{-4} laws intercept, this definition can also be used for a broad class of aerogels. In particular, q_χ is the only quantitative crossover value for materials with polydisperse, or poorly defined primary particles, such as those studied in references [7, 8]. For our colloidal samples, the values of $q_\chi\, r_0$, given in table I, are sample independent for aerogels belonging to the same series, but vary slightly from one series to the other. This shows that q_χ can only be considered as an indication from which a precise value of the average particle size cannot be deduced.

In conclusion, the precise knowledge of the form, size and polydispersity in these materials has allowed a quantitative study of the various features observed in SANS data. The observations call for further studies, in particular for numerical calculations of $g(r)$ in the r_0 range on realistic aggregation models.

Acknowledgments.

The authors gratefully acknowledge the invaluable help of Prof. J. Teixeira with the SANS experiment.

References

[1] GUINIER A., Théorie et Technique de la Radiocristallographie (Dunod, Paris, 1956).
[2] DE GENNES P. G., Scaling Concepts in Polymer Physics (Cornell U. P., Ithaca, 1979).
[3] SCHMIDT P. W., *J. Appl. Cryst.*, to be published (1991).
[4] TEIXEIRA J., in On Growth and Form, H. E. Stanley and N. Ostrowsky Eds. (Martinus Nijhoff, Dordrecht, 1986) p. 145.
[5] FRELTOFT T., KJEMS J. K. and SINHA S. K., *Phys. Rev. B* **33** (1986) 269.
[6] CHEN S. H. and TEIXEIRA J., *Phys. Rev. Lett.* **57** (1986) 2583.
[7] SCHAEFER D. W., MARTIN J. E. and KEEFER K. D., *Phys. Rev. Lett.* **56** (1986) 2199.
[8] VACHER R., WOIGNIER T., PELOUS J. and COURTENS E., *Phys. Rev. B* **37** (1988) 6500.
[9] DIMON P., SINHA S. K., WEITZ D. A., SAFINYA C. R., SMITH G. S., VARADY W. A. and LINDSAY H. M., *Phys. Rev. Lett.* **57** (1986) 595.
[10] KISTLER S. S., *J. Phys. Chem.* **36** (1932) 52.
[11] ZERNIKE F. and PRINS J. A., *Z. Phys.* **41** (1927) 184.
[12] For a more detailed analysis of this problem, see JULLIEN R., in this issue.
[13] MEAKIN P., *Phys. Rev. Lett.* **51** (1983) 1119.
[14] KOLB M., BOTET R. and JULLIEN R., *Phys. Rev. Lett.* **51** (1983) 1123.